AGU PUBLICATIONS

JGR

Journal of Geophysical Research: Atmospheres

RESEARCH ARTICLE

10.1002/2015JD023176

Key Points:

- Polluted MSC remain as closed cells for longer time
- Continents can act as huge aerosol sources and form "continent tracks"
- Potentially hitherto unrecognized large negative RF over large area and time

Supporting Information:

- Supporting Information S1
- Movie S1
- Movie S2
- Movie S3
- Movie S4

Correspondence to:
T. Goren,
tom.goren@mail.huji.ac.il

Citation:
Goren, T., and D. Rosenfeld (2015), Extensive closed cell marine stratocumulus downwind of Europe—A large aerosol cloud mediated radiative effect or forcing?, *J. Geophys. Res. Atmos.*, *120*, doi:10.1002/2015JD023176.

Received 27 JAN 2015
Accepted 22 MAY 2015
Accepted article online 1 JUN 2015

Extensive closed cell marine stratocumulus downwind of Europe—A large aerosol cloud mediated radiative effect or forcing?

Tom Goren[1] and Daniel Rosenfeld[1]

[1]The Hebrew University of Jerusalem, Institute of Earth Sciences, Jerusalem, Israel

Abstract Marine stratocumulus clouds (MSC) cover large areas over the oceans and possess super sensitivity of their cloud radiative effect to changes in aerosol concentrations. Aerosols can cause transitions between regimes of fully cloudy closed cells and open cells. The possible role of aerosols in cloud cover has a big impact on the amount of reflected solar radiation from the clouds, thus potentially constitutes very large aerosol indirect radiative effect, which can exceed 100 $\mathrm{W\,m^{-2}}$. It is hypothesized that continentally polluted clouds remain in closed cells regime for longer time from leaving continent and hence for longer distance away from land, thus occupying larger ocean areas with full cloud cover. Attributing this to anthropogenic aerosols would imply a very large negative radiative forcing with a significant climate impact. This possibility is confirmed by analyzing a detailed case study based on geostationary and polar-orbiting satellite observations of the microphysical and dynamical evolution of MSC. We show that large area of closed cells was formed over the northeast Atlantic Ocean downwind of Europe in a continentally polluted air mass. The closed cells undergo cleansing process that was tracked for 3.5 days that resulted with a rapid transition from closed to open cells once the clouds started drizzling heavily. The mechanism leading to the eventual breakup of the clouds due to both meteorological and aerosol considerations is elucidated. We termed this cleansing and cloud breakup process maritimization. Further study is needed to assess the climatological significance of such situations.

1. Introduction

Marine stratocumulus clouds (MSC) occur in two main cloud regimes, open and closed cells, which differ significantly in their cloud cover [*Agee et al.*, 1973; *Atkinson and Zhang*, 1996]. The cloud cover is nearly 100% in the closed cells, whereas the open cells have cloud cover that is typically less than 65% [*Goren and Rosenfeld*, 2014; *Wood and Hartmann*, 2006; *Wood et al.*, 2011]. Observational studies have shown that the closed cells have high aerosol and droplet concentrations compare to open cells [*Wang and Feingold*, 2009; *Wood et al.*, 2011]*Wood et al.*, 2008, 2011]. Closed MSC open when the droplet concentration (N_d) is low enough to allows heavy drizzle that further causes positive feedback that trigger rapid transition from closed to open cells [*Gerber*, 1996; *Rosenfeld et al.*, 2006; *Rosenfeld et al.*, 2012]. The occurrence of heavy drizzle can be inferred by the cloud top effective radius (r_e). An r_e that exceeds ~15 μm implies an efficient collisions and coalescences that causes significant rain rates [*Rosenfeld et al.*, 2012], i.e., sufficient for fast scavenging of the aerosols and for creating cold pools and gust fronts that organize the convection in the form of open cells [*Feingold et al.*, 2010; *Terai and Wood*, 2013]. *Freud and Rosenfeld* [2012] have shown that in nonprecipitating clouds the cloud depth in which the r_e reaches a given value increases linearly with N_d. This means that aerosols that increase N_d in a cloud also increase the cloud depth for reaching r_e of 15 μm, thus delaying the initiation of rain to greater heights, which might be greater than the actual cloud top height. In such case the breaking of closed cells into open cells can be prevented.

The effect of clouds on the planetary radiation budget is named cloud radiative effect (CRE), which is defined as the difference in the top of the atmosphere and surface radiation budgets with clouds versus clear-sky situation at the location of the cloud. It is known that aerosols can change the albedo of the clouds [e.g., *Albrecht*, 1989; *Twomey*, 1977] and cause aerosol CRE, which is the change in CRE due to a given change in aerosols, that may be natural or anthropogenic. Aerosol radiative forcing (RF) is defined according to the Intergovernmental Panel on Climate Change [*Field et al.*, 2014] as the difference in the energy fluxes caused by anthropogenic aerosols. Therefore, the same aerosol effect on cloud radiative properties would be considered as CRE if the aerosols are natural or RF if the aerosols are anthropogenic.

The large sensitivity of the MSC regimes to aerosols is demonstrated in *Goren and Rosenfeld* [2012] who showed that ship emissions can convert broken MSC into closed MSC along with a large increase in the reflected solar radiation. In their study the increased reflected solar radiation could be directly related to the effect of anthropogenic aerosols from ship emissions. Therefore, the change in CRE due to the ship emissions can be referred as RF. *Goren and Rosenfeld* [2014] have shown that the differences in CRE between open and closed cells can be larger than $-100\,\mathrm{W m^{-2}}$, depending on the season and latitude. The attribution of this potentially large CRE can be partitioned to changes in cloud cover, droplets size (i.e., Twomey effect [*Twomey*, 1977]), and cloud water path (LWP). It was found that the combination of horizontal cloud cover effect and the vertical cloud cover effect (i.e., LWP) contributes ~75% of the CRE, while the Twomey effect contributes the remaining ~25% [*Goren and Rosenfeld*, 2014]. In the case where the aerosols that keep the MSC closed are anthropogenic, the CRE can be considered as RF. Other satellite studies [*George and Wood*, 2010; *Kaufman et al.*, 2005; *Lebsock et al.*, 2008; *Sekiguchi et al.*, 2003] also showed that most of the top of the atmosphere CRE of shallow clouds was caused by an increase in the cloud cover and LWP rather than in the Twomey effect. *Kaufman et al.* [2005] showed that the enhanced solar reflectance that was associated with increased aerosol optical depth was contributed mostly by the cloud cover effect, which was 3–5 times larger than the Twomey effect. *George and Wood* [2010] showed that the variability in cloud fraction, LWP, and N_d explains on average roughly 1/2, 1/3, and 1/10 of the spatial variance of the area mean albedo that was accounted for by these variables, respectively, but they could not rule out the effects of meteorology in these changes.

Many observational and modeling studies show evidence that precipitation plays a key role in the transition from closed to open cells regime [*Stevens et al.*, 2005; *Sharon et al.*, 2006; *Wood et al.*, 2008, 2011; *Terai et al.*, 2014] and that precipitation rates decrease as N_d increases for the same LWP [*Lu et al.*, 2007; *Wood*, 2005]. Aerosols have been even shown to be able to convert open to closed cells regime [*Goren and Rosenfeld*, 2012; *Feingold et al.*, 2015]. This implies that it is quite possible that large quantities of anthropogenic pollution that come from continents can prevent closed cells from breaking up by delaying the onset of heavy drizzle. Aerosols can be transported to the marine boundary layer (MBL) through the MBL or penetrate into the MBL from above. *Allen et al.* [2011] have shown a significant coast to ocean gradient in aerosols during VAMOS Ocean-Cloud-Atmosphere-Land Study Regional Experiment measurements and that the aerosols can be attributed to anthropogenic source. Previous studies [*Allen et al.*, 2011; *George et al.*, 2013; *Saide et al.*, 2012; *Schwartz et al.*, 2002; *Twohy et al.*, 2009; *Yang et al.*, 2011] have already shown the impact of continental aerosols that are transported from continents on the cloud radiative properties of marine clouds, emphasizing the potential effect of anthropogenic aerosols on the CRE. However, they related the observed radiative impacts mainly to the Twomey effect [*Twomey*, 1977], due to increased N_d, without considering possible aerosol-induced regime changes. In this study we focus on the aerosol-induced regime changes and further show that closed cells that form within continental air mass can remain in the closed cells regime up to 3 days before breaking to open cells and to induce large radiative effect, mainly due to the cloud cover effect. We show that large areas of closed cells that are frequently seen over the subtropical oceans can be, at least partly, attributed to anthropogenic aerosols. If anthropogenic aerosols are responsible to the longer life time of the observed closed cells, their large cloud radiative effect needs to be considered as cloud radiative forcing.

The data and the methodology are described in section 2. Section 3 provides a detailed satellite analysis of the cloud evolution and cloud properties, analysis of the possible anthropogenic signature, and a documentation of the closed to open cells process. Section 4 includes the discussion of the results and conclusions.

2. Data and Methodology

The evolution of the MSC was analyzed based on observations taken every hour by the Spinning Enhanced Visible and Infrared Imager (SEVIRI) instrument on board the Meteosat Second Generation (MSG). We used day and night microphysical RGB (red-green-blue) composite images to interpret the cloud microphysical properties [*Lensky and Rosenfeld*, 2008]. In the day-microphysics RGB the 0.8 μm reflectance modulates the red as a measure for the cloud optical depth (stronger red means thicker clouds with more water), the 3.9 μm solar reflectance modulates the green and is a measure of the cloud particle size (stronger green means smaller droplets), and the 10.8 μm cloud tops brightness temperature modulates the blue (stronger blue means warmer cloud tops). In the night microphysical RGB, brightness temperature difference (BTD) of 12.0–10.8 μm modulates the red as a measure for the clouds' opaqueness (stronger red means more opaque or optically thick cloud), BTD of 12.0–3.9 μm modulates the green and is sensitive to particle size (stronger green means smaller droplets, as for day microphysics), and the 10.8 μm cloud top brightness temperature modulates the blue (stronger blue means warmer clouds, as for day microphysics). SEVIRI cloud products were taken from the European Organisation for the Exploitation of Meteorological Satellites (EUMETSAT's) Satellite Application Facility on Climate Monitoring (http://www.cmsaf.eu/bvbw/appmanager/bvbw/cmsafInternet). SEVIRI also provided us with atmospheric motion vector (AMV) product that was used to identify cloud motion (http://www.eumetsat.int/website/home/Data/Products/Atmosphere/index.html). In addition, we used Hybrid Single-Particle Lagrangian Integrated Trajectory Model (HYSPLIT) to generate back trajectories of air parcels [*Draxler and Rolph*, 2015; *Rolph*, 2015].

Detailed cloud properties at 1 km spatial resolution were retrieved from the Moderate Resolution Imaging Spectroradiometer (MODIS) detector on board Terra and Aqua satellites. The cloud microstructure was depicted from MODIS level 2 cloud products collection 5.1 [*Platnick et al.*, 2003]. Cloud droplet concentrations, N_d, was calculated based on the method of *Szczodrak et al.* [2001], as used by *Goren and Rosenfeld* [2014]. It should be noted that retrieval errors of the satellite cloud retrievals may bias the microphysical analysis. Such errors are minimized over homogeneous cloud fields as closed cells [*Zhang and Platnick*, 2011], which are analyzed in this study.

Cloud top heights were retrieved from the Cloud Aerosol Lidar with Orthogonal Polarization (CALIOP) level 2 cloud layer product (version 3.01). Below 8 km CALIOP resolves cloud layers with vertical resolution of 30 m sampled along the orbit every 333 m. Cloud and rain reflectivity were derived from the observations of the 94 GHz cloud profiling radar (CPR) onboard CloudSat and were obtained from level 2B-Geoprof [*Marchand et al.*, 2008]. The CPR provides radar reflectivity with vertical profiles spaced horizontally every 1.1 km and vertically sampled at 240 m intervals with minimum detectable signal of −28 dBZ. Scenes that were identified by MODIS aqua were collocated with observation of CALIOP and CloudSat to provide the cloud top heights and a measure for the rain rates. As the three satellites are part of the A-Train constellation, the observations from the different satellites are only few minutes apart.

Sulfate mixing ratio was obtained from the Goddard Chemistry Aerosol Radiation and Transport (GOCART) model [*Chin et al.*, 2014]. Ground-based measurements of carbon monoxide concentration at 5 m above ground level from Mace-Head atmospheric research station were taken from http://agage.eas.gatech.edu/data_archive/agage/gc-md/complete/macehead/.

Reanalysis and meteorological observations including sea surface temperatures (SST) were taken both from the National Centers for Environmental Prediction-National Centers for Atmospheric Research (NCEP/NCAR) (http://www.esrl.noaa.gov/psd/data/gridded/data.ncep.reanalysis.html) and the European Centre for Medium-Range Weather Forecasts (ECMWF) (http://www.ecmwf.int/). NCEP/NCAR is evaluated on 2.5° grid, while ECMWF on 0.5°. The CRE and its partitioning were calculated based on the method of *Goren and Rosenfeld* [2014].

3. Detailed Description of a Case Study

In this section we present a detailed analysis of a case study, in which large area of closed cells formed downwind the British Islands and Western Europe. We show that the closed cells formed within an air mass that contained anthropogenic signature. In addition to this case we have found two other cases with a similar behavior and extent. In the supporting information one can find satellite sequence animations for the presented case study (Movies S1 and S2 in the supporting information) as well as for two additional similar cases (Movies S3 and S4 in the supporting information). We chose the case of January 2010 because it allowed a continues visual and microphysical documentation without disturbance of high level clouds. In addition, data from the A-Train (MODIS, CALIPSO, and CloudSat) were best available for this case. It should be noted that we have observed additional cases that show similar behavior of closed cells that form downwind of Europe, but those need further analysis, and thus, they are not shown here.

3.1. Synoptic Background and Sea Surface Temperature Variation

Sea level pressure and 500 hPa geopotential height are shown in Figure 1. A stationary high-pressure system accompanied with an upper level ridge was established in the north-eastern Atlantic Ocean. The synoptic

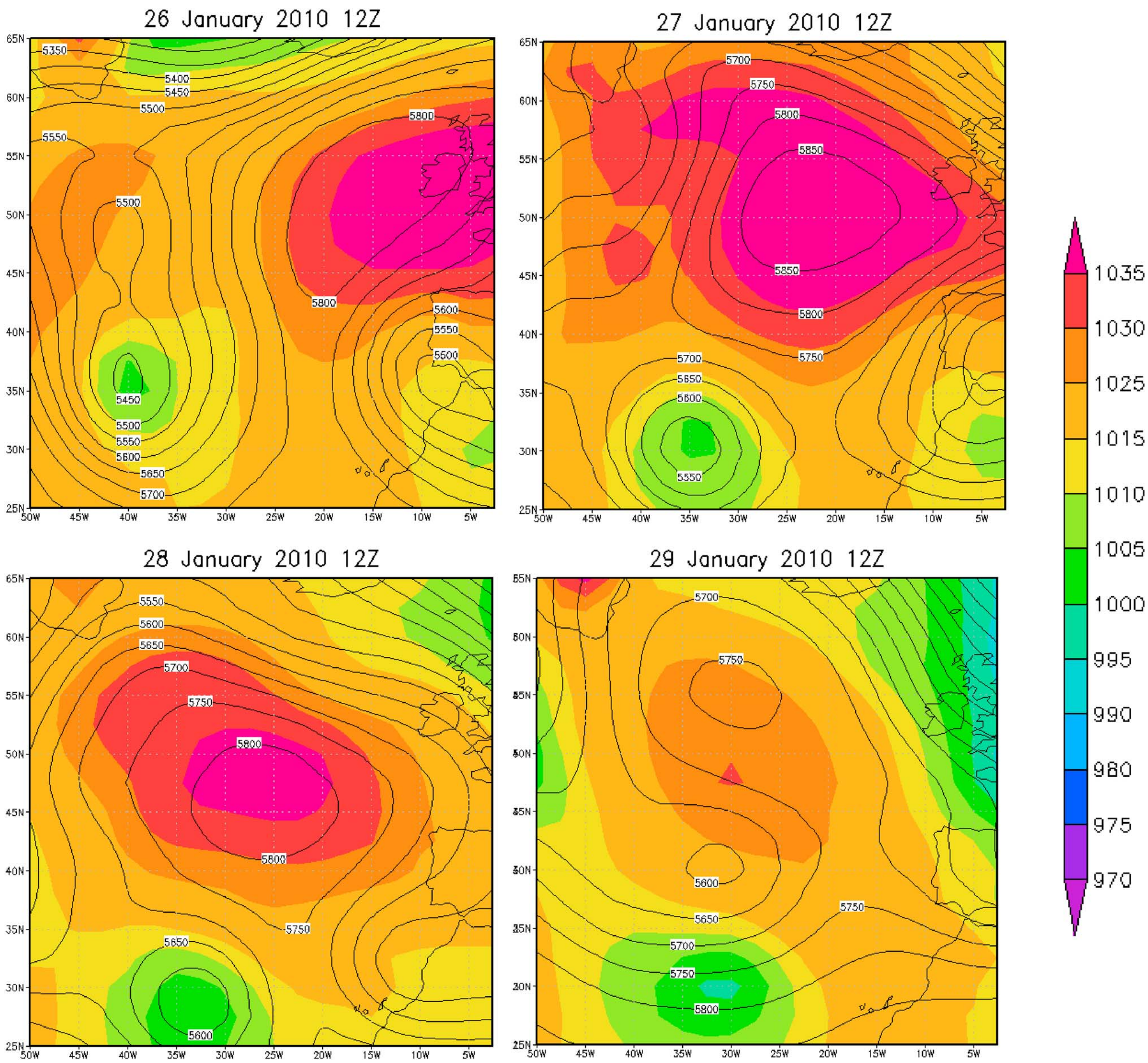

Figure 1. Sea level pressure (mb) in color and 500 mb geopotential height (m) in black contours for 26–29 of January 2010 12Z. High-pressure system both at the surface and 500 hPa is seen over the area where the marine stratocumulus clouds were observed.

configuration caused easterly winds that transported continental air from Europe into the Atlantic Ocean. MSC favor such condition of high pressure both at surface and upper levels, and its stationary state in the following 3 days allowed a relatively long period of time to study the clouds evolution while keeping the synoptic conditions similar. Figure 2 shows sea surface temperature (SST) for the area where the MSC were observed. A gradual meridional temperature gradient can be seen.

3.2. Satellite Analysis of the Cloud Evolution

Figures 3a–3h shows a 3.5 day sequence of the satellite images of the clouds, using day and night RGB rendering. The RGB color scheme is described in section 2. The black line represents the interface between the clouds that formed in the continental air (hereafter continental clouds) to those that exist in the maritime air (hereafter maritime clouds). The closed cells east to the interface line are associated with the advected air from western Europe, as illustrated by the arrows that represent the flow direction around the anticyclone center. The maritime clouds formed over the ocean in an air mass that was possibly

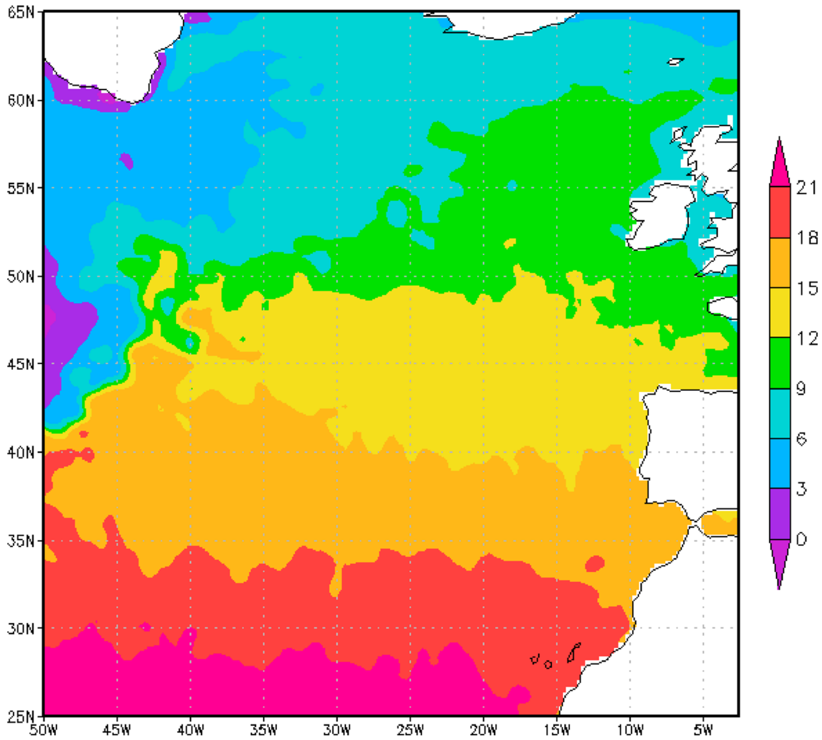

Figure 2. Sea surface temperature (°C) over the north east Atlantic Ocean on 28 January 2010. A moderate meridional SST gradient is seen.

originated in North America (see section 3.3) and are defined as such just in a relative sense. An animated sequence of the satellite images with 1 h intervals is provided in Movies S1 and S2.

In Figure 3a the yellow (i.e., having small r_e) clouds move westward from the British Inlands and northern France driven by the high pressure that is centered over Ireland and the low pressure that is centered over southern Spain. The clouds move along with the anticyclonic circulation westward into the ocean, pushing westward the clouds that exist within the maritime air mass. The difference between the air masses can be seen by the cloud r_e and N_d, so that r_e is larger and N_d is lower in the clouds that exist in the maritime air mass (see section 3.4 for a detailed analysis of the cloud properties). For comparison, MODIS r_e over the continental clouds is less than 10 µm, while the r_e of the maritime clouds is about 15 µm.

In the following night (Figure 3b) the continental clouds are already covering large area over the ocean. Note the orientation of the interface between the maritime and the continental clouds as it rotates anticyclonically, indicating that both cloud areas are subject to similar meteorology. The maritime closed cells were observed to break during the night as can be seen in the following day just north of the interface line (Figure 3c). The purple colors of the clouds and their breakup imply that these clouds have larger cloud drops and that they are drizzling relatively heavily. This is confirmed by MODIS r_e that shows r_e that is larger than 15 µm over the broken clouds. The large deck of the continental closed cells on the other hand still has r_e that is less than 15 µm (not shown). This large closed cells area can be comparable to a huge ship track, in which the ship in this case is western Europe.

The rotation of the clouds and the breakup of the maritime closed cells continued in the following 24 h (Figures 3d and 3e). It is interesting that at this point of the sequence (Figure 3e) the interface has rotated anticyclonically 180°, so that the position of the open and closed cells are in opposite to the expected logic if one looked at it without knowledge of its history. The continental closed cells are located on the side that is far from land, while the pristine area with the maritime open cells is in the air mass that is closer to land. Note that the rotation of the anticyclone brings closed cells that begin to break both to warmer and colder SST (Figure 2). This implies that changes in SST cannot possibly explain the changes in

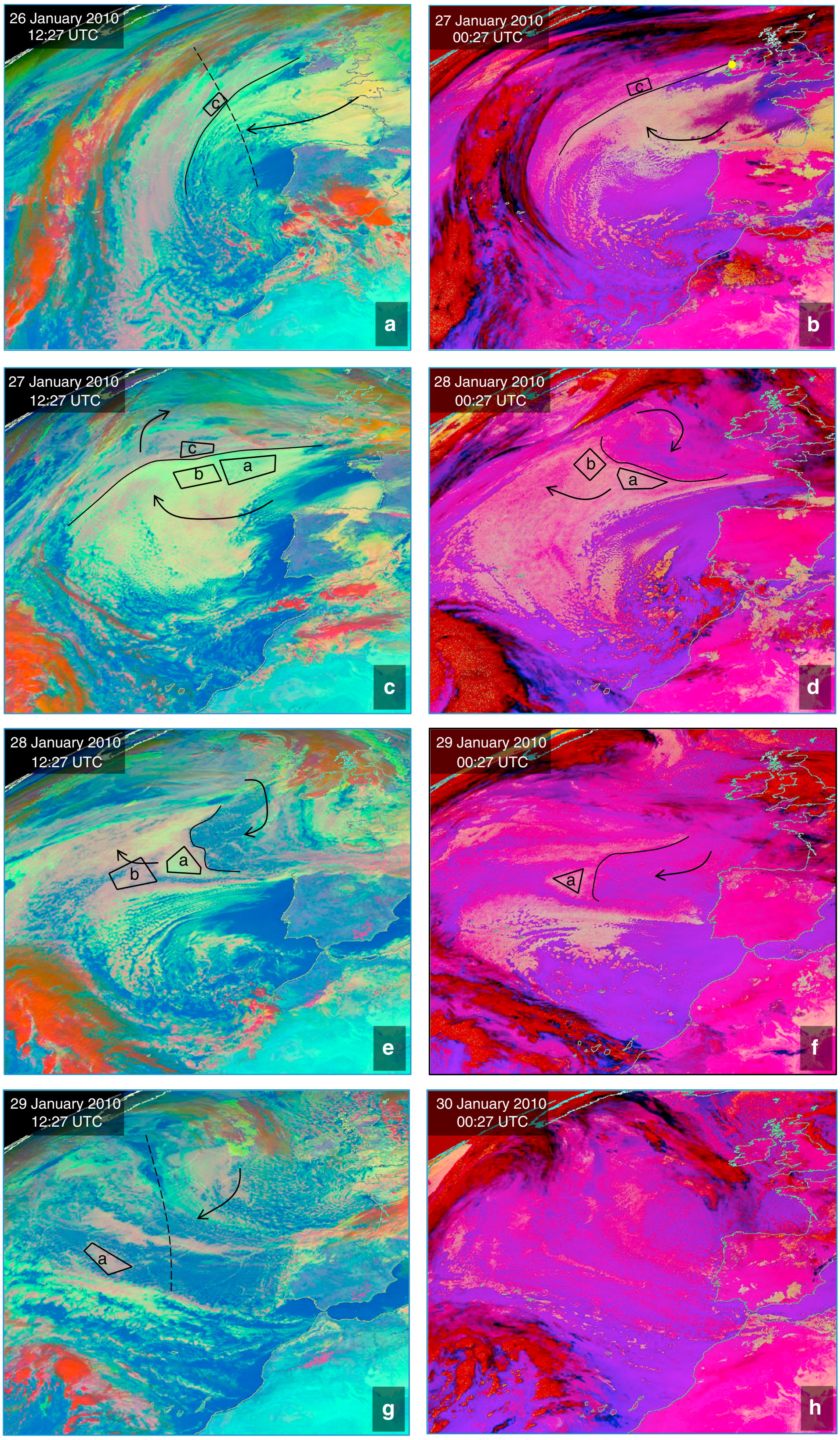
26 January 2010
12:27 UTC
c
a
27 January 2010
00:27 UTC
c
b
27 January 2010
12:27 UTC
c
b
a
c
28 January 2010
00:27 UTC
b
a
d
28 January 2010
12:27 UTC
b
a
e
29 January 2010
00:27 UTC
a
f
29 January 2010
12:27 UTC
a
g
30 January 2010
00:27 UTC
h

Figure 3

the cloud regimes and that other factor rather than SST changes are probably more dominant in the process of regime change. Also, note that the interface is located at the rotation axis of the anticyclone, indicating that similar meteorology control the closed and open cells.

The drizzle within the open cells that exist in the maritime air mass east of the interface line (Figure 3e) further cleans the clouds and produces positive feedback for keeping them in the open cells regime [*Rosenfeld et al.*, 2006]. The purple color of the clouds indicates larger cloud drops and thus more pristine air. An evidence for the clean environment is ship tracks that can be seen in the open cells area to the east of the interface line.

In the following 24 h (Figures 3f and 3g) the continentally related closed cells continued to break in areas where the r_e exceeds the threshold of 15 μm, resulting in patches of closed cells embedded in an area of open cells (see section 3.4 for a detailed analysis of the cloud properties). Ship tracks can be seen across the open cells, indicating the super clean environment, which is the last stage of the cleansing process of the continental clouds. We termed this process maritimization, as the clouds microphysics change from continentally polluted to pristine marine, together with the transition from closed to open cells and a significant reduction in the cloud cover. It should be noted, however, that the maritimization process can have other pathways and that here we explore one pathway that occurs when the boundary layer contains a stratocumulus deck.

3.3. Evidence for Anthropogenic Aerosols in the Continental Closed Cell

Evidence for anthropogenic aerosols in the continental closed cells was available from two sources: (1) modeled sulfate mixing ratio produced by the Goddard Chemistry Aerosol Radiation and Transport (GOCART) model [*Chin et al.*, 2014] and (2) in situ measurements from Mace-Head station that is located on the western coast of Ireland.

Anthropogenic sources are the main contributor to sulfate in the MBL over most continental areas [*Benkovitz et al.*, 1996; *Chin and Jacob*, 1996; *Spiro et al.*, 1992]. Sulfates can act as cloud condensation nuclei (CCN) that modify the cloud microphysics and albedo [*Boucher and Lohmann*, 1995; *Twomey*, 1974]. Under suitable conditions sulfates can be advected outside the continents into the pristine oceans, as observed in the case study presented here. Figure 4 shows sulfate mixing ratio at the surface over the north east Atlantic ocean for the same time steps as in Figure 3. It can be seen that the movement of areas with higher and lower sulfate mixing ratios correspond to the continental-maritime clouds' interface movement that is described in section 3.2 and shown in Figure 3.

Note the slightly higher sulfate mixing ratios marked by black dots in Figures 4a and 4b. In this area the maritime closed cells exists (see Figures 3a and 3b). Tracking back the origins of this area shows that the air mass is originated in North America 5–7 days earlier (not shown). This suggests that the maritime closed cells may have been created in an old continentally north American polluted air mass.

In situ observation of the carbon monoxide (CO) that indicates anthropogenic signature was available from the monitoring station of Mace-Head in the western coast of Ireland and is shown in Figure 5. The northern edge of the interface line between the continental and the maritime closed cells have passed over the monitoring station during the night between the 26 and 27 of January (see Figure 3b; Mace-Head station is marked by a yellow circle). A sudden change in the air composition was observed as the interface line between the two air masses passed over the monitoring station. The CO was observed to decrease

Figure 3. The cloud evolution as seen by the MSG geostationary satellite. The sequence covers the period of 26–30 January 2010 every 12 h. (a, c, e, and g) Plots occur at local noon and therefore rendered with the "day microphysical" color scheme (the RGB color scheme is described in section 2). In this scheme water clouds with small drops appear yellow and water clouds with large drops appear pink. The ship tracks within the open cells (Figures 3e and 3g) appear more conspicuously as yellow lines within the purple areas. (b, d, f and h) Plots occur at local midnight and therefore rendered with the "night microphysical" color scheme. In this scheme water clouds with small drops appear white and water clouds with large drops appear purple. The red clouds are composed of ice. The ocean is colored dark blue. The white areas are closed cells with small cloud drops. The arrows represent the flow direction around the anticyclone center. The black line represents the interface between the maritime and continental air masses as inferred by the r_e of the clouds and by the MSC regime. The polygons mark the closed cells area that were tracked and analyzed for the macro and microphysical evolution of the clouds (see section 3.5.1 and Figure 8). The yellow point in Figure 3b is where the monitoring station Mace-Head is located. The dashed lines in Figures 3a and 3g represent the A-Train satellite track (refer to Figures 6 and 7).

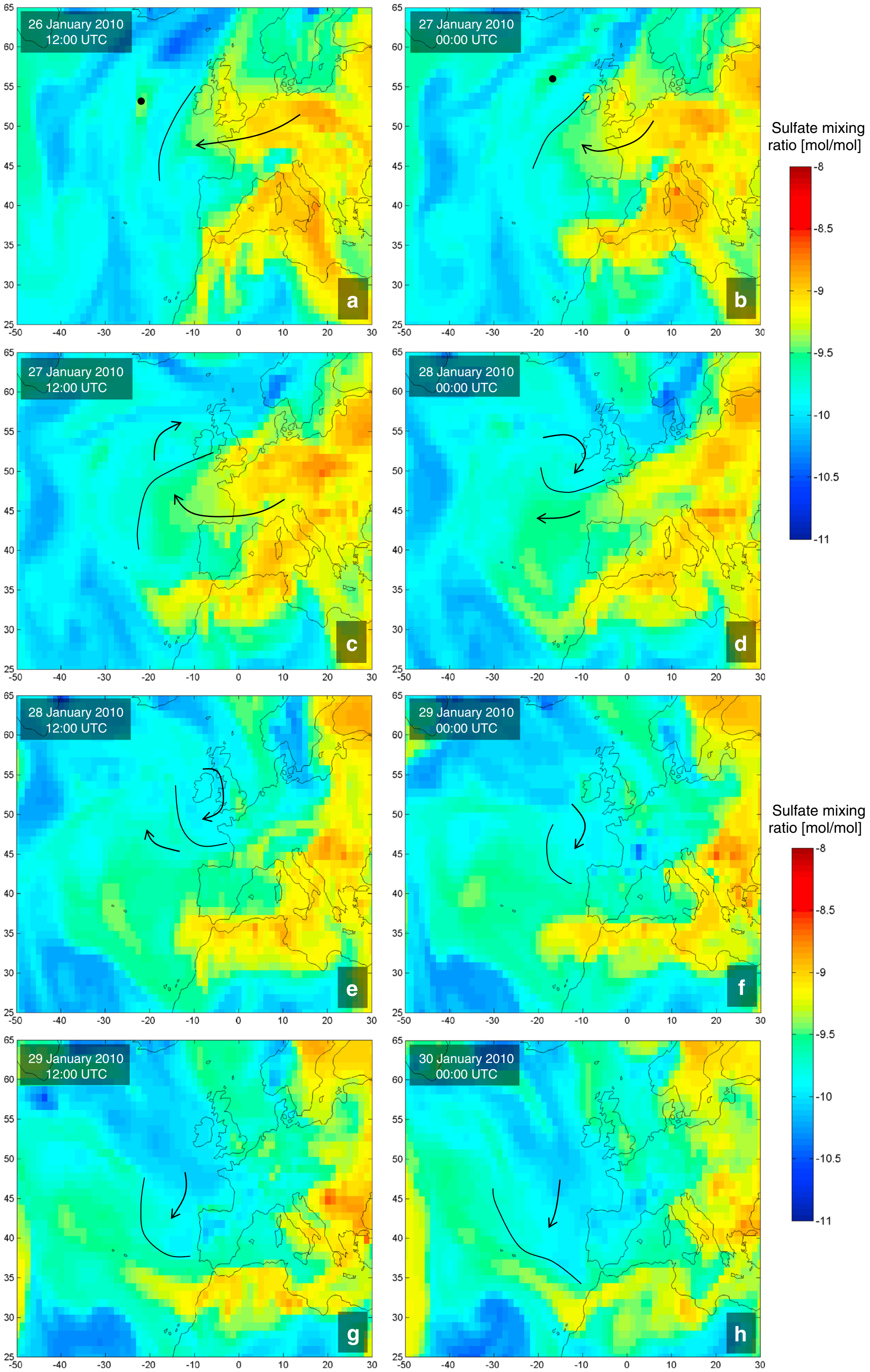
26 January 2010
12:00 UTC
a
27 January 2010
00:00 UTC
b
27 January 2010
12:00 UTC
c
28 January 2010
00:00 UTC
d
28 January 2010
12:00 UTC
e
29 January 2010
00:00 UTC
f
29 January 2010
12:00 UTC
g
30 January 2010
00:00 UTC
h
Sulfate mixing
ratio [mol/mol]
-8
-8.5
-9
-9.5
-10
-10.5
-11

Figure 4

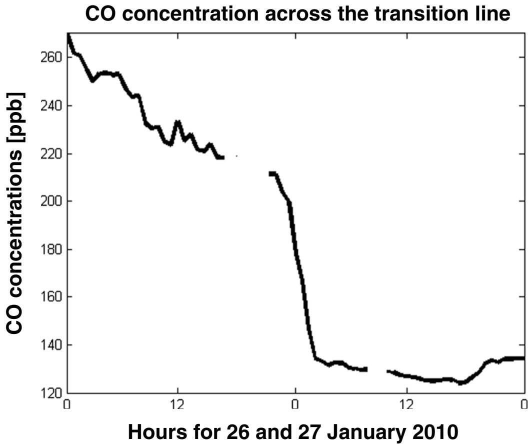

Figure 5. Carbon Monoxide concentrations (ppb) taken from the monitoring station in Mace-Head for the time in which the interface line between the maritime and the continental closed cells passed over the site (see Figure 3b). The gap in the line means no data. An abrupt decrease in the CO concentrations is seen, implying the role of anthropogenic aerosols in the continental closed cells.

abruptly from concentrations of about 220 ppb under the continental closed cells to about 130 ppb under the marine closed cells (Figure 5).

The above analysis implies that the air mass experienced an anthropogenic influence that can potentially explains the microphysical differences between the continental and maritime cloud areas and the larger cloud cover in the continental air mass. The microphysical differences are further discussed in the following section.

3.4. Detailed Analysis of Cloud Properties

The microphysical and macrophysical differences across the interface zone between the continental and the maritime closed cells were analyzed by CALIPSO, CloudSat, MODIS r_e, and N_d. Note that overlap between CALIPSO, CloudSat, and MODIS is available only for aqua satellite. Figures 6 and 7 show the collocated data from the three instruments for the available overlaps.

Figure 6 shows the early stage when closed cells start to form within the continental air mass as the continental air passed over the ocean. The center white line in Figures 6c–6e is shown as the dashed line in Figure 3a. The cloud top heights (Figure 6a and 6b) along the two sides of the interface line indicate the inversion base, which is determined by the large scale meteorology. The inversion height (also MBL depth) can be seen to lower toward the high pressure that is centered around 49°N (Figure 1) and then to rise again northward. Figure 6b also shows the calculated cloud base height, which is calculated based on MODIS LWP and adiabatic cloud assumption with estimated cloud base temperature and pressure (given warm and shallow clouds as analyzed here, inaccuracy of cloud base temperature and pressure have minor effect on the cloud depth). The cloud base calculations take into account three pixels along each side of the A-Train track (indicated by the white horizontal line in Figures 6c–6e), from which only pixels with optical thickness larger than 10 are included. These pixels are assumed to represent the deepest and most active clouds that are also more closely satisfying the adiabatic assumption. Note that the continental and maritime cloud interface is located at the center of the high pressure (around 49° in Figure 6) and that there is no abrupt change in the cloud top or base heights, implying that similar meteorology controls both sides of the interface line. Figure 6c shows that the cloud depth overlaid the r_e imagery. It can be seen that cloud depth increases in areas where CloudSat shows higher reflectivity within the maritime closed cells (around latitude 50.5°; Figure 6b). This is in accordance with the r_e threshold of 15 μm for significant drizzle rates that predicts the closed cells breakup few hours later. At the continental side (left to the interface line in Figure 6c) the r_e is below 10 μm with no measurable radar reflectivity. Figures 6d and 6e show N_d that is significantly higher within the continental closed cells (~400 cm^{-3} in the continental closed cells compare to ~80 cm^{-3} in the maritime closed cells). This support the continental nature of the air mass with the elevated aerosol concentrations, in which the continental closed cells exists.

Figure 7 is for the final stage, when most of the continental closed cells broke to open cells and only few patches of closed cells remained. The center white line in Figures 7c–7e is shown as the dashed line in Figure 3g. At this stage most of the additional CCN were scavenged and thus the decrease of N_d can be

Figure 4. (a–h) Sulfate mixing ratio (mol/mol) shown in a logarithmic scale for the same times as in Figure 3. The black line represents the interface between the maritime and continental air masses as inferred by the sharp gradient in the sulfate mixing ratio. The arrows represent the flow direction around the anticyclone center. The yellow point in Figure 4b is where the monitoring station Mace-Head is located. The black point symbols the location of Figure 4c in Figure 3. Note the different map projection relative to Figure 3.

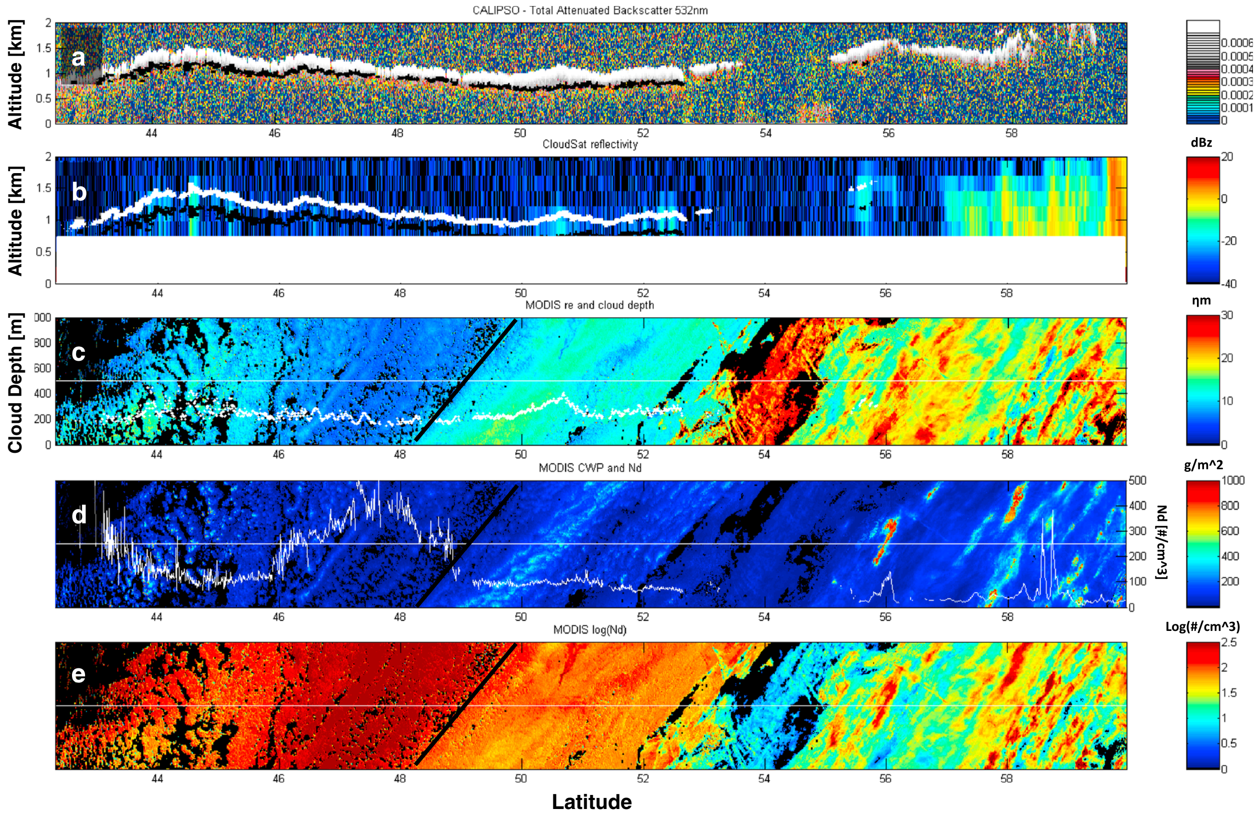

Figure 6. Collocation of data retrieved from CALIPSO, CloudSat, and MODIS-Aqua for 26 January 2010 near 14:10 UTC. (a) CALIPSO 532 nm attenuated backscatter. The top of the white line represents the cloud top heights; the black line represents the calculated cloud base heights. (b) CloudSat reflectivity with CALIPSO cloud top height (white line) and calculated cloud base heights (black line), data below 750 m is screened due to ground noise. (c) MODIS r_e with cloud depth (white line). (d) MODIS LWP with N_d (white line). (e) The logarithmic of N_d. The white horizontal lines in Figures 6c–6e represent the ground track of CALIPSO and CloudSat (that is also shown by the dashed line in Figure 3a). The black diagonal line represents the interface between the maritime and the continental closed cells. Note that cloud depth does not show a sharp change across the sides of the interface line. Little reflectivity is observed within the maritime closed cells right of the interface line (~50.5°), as also implied by the r_e that is nearly 15 µm. Also note the difference in N_d across the sides of the interface line.

accelerated further through collisions and coalescences processes. This is in fact the transition from the updraft limited to the aerosol limited regime, as defined by *Reutter et al.* [2009]. The patch of closed cells that is seen in Figure 7 around latitude 42.5° is a remnant of the continental closed cells that formed 3 days earlier. The drizzle is weaker in its core compare to its edges (as inferred by CloudSat reflectivity in Figure 7b), indicating that mixing between the closed cells and the super clean air that surrounds it may be responsible for the initiation of drizzle and the subsequence breakup.

The existence of open and closed cells in such proximity implies that similar meteorology governs both areas. In addition, the low variation of the SST (Figure 2) means that SST variations are not likely to explain the different regimes. The role of meteorology, SST changes, and N_d on the transition from closed to open cells is further analyzed in the following section.

3.5. Factors Controlling the Transition From Closed to Open Cells

In order to characterize the transition from closed to open cells we performed a Lagrangian analysis for tracking the closed cells along the days until their breakup and documented the microphysical and meteorological evolution. The microphysical parameters were retrieved from the SEVIRI cloud product while the meteorological parameters from ECMWF reanalysis. The tracking of defined cloud areas was performed visually using the MSG satellite, provided by its high temporal resolution of 15 min. Because the size of the tracked areas constantly changes it makes automatic tracking methods too complicated. Therefore, for the need of this study we did not use any automatic tracking methods. However, we did use HYSPLIT back trajectory analysis to confirm our visual tracking.

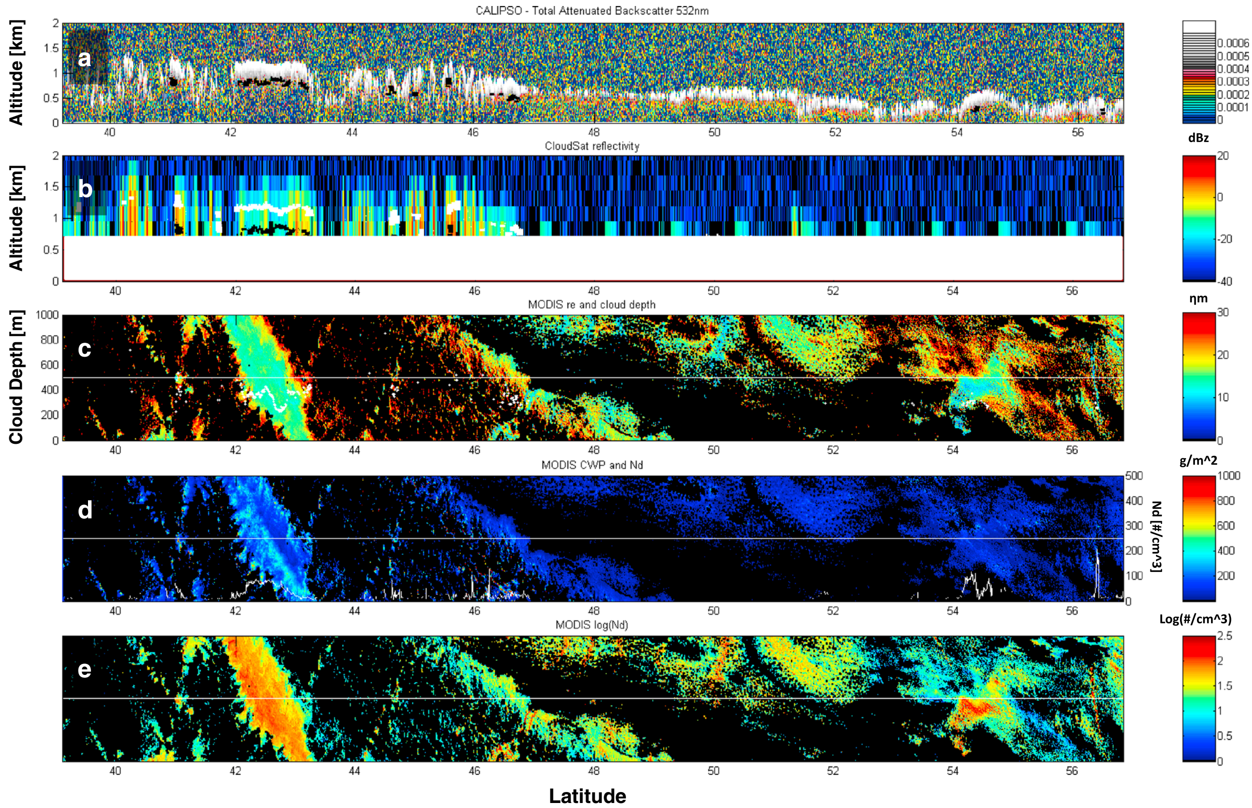

Figure 7. Same as Figure 6 but for 29 January 2010 near 14:40 UTC. The ground track of CALIPSO and CloudSat is shown by the dashed line in Figure 3g At this stage all of the maritime and most of the continental closed cells have broken to open cells. Only few patches of continental closed cells remained closed (see the closed cells patch around latitude 42.5°). The closed cells r_e is nearly 15 μm and have small reflectivity compare to the open cells around.

An adiabatic parcel model was used to calculate the adiabatic cloud LWP and r_e of the tracked cloud elements for each time step, based on the cloud base temperature, height, and pressure. In order to calculate the adiabatic r_e we first calculated the droplet mean volume radius, r_v, by dividing the adiabatic LWP by the MODIS retrieved N_d. Based on the relation between r_e and r_v, which is on average 1.08 [*Freud and Rosenfeld*, 2012] we calculated the adiabatic r_e as a function of height above cloud base.

We further define two cloud depths, the geometrical cloud depth (D) and the theoretical critical cloud depth (D_c), which is the cloud depth at which the cloud top r_e reaches 15 μm (i.e., initiation of significant drizzle). It should be noted that while observational and modeling studies have shown that rain is initiated when r_e near cloud tops is around 12–14 μm [*Freud and Rosenfeld*, 2012; *Gerber*, 1996; *Rangno and Hobbs*, 2005; *Rosenfeld et al.*, 2012], here we use r_e of 15 μm. This is so because MODIS retrieved r_e was found to overestimate the in situ r_e by about 1–2 μm around r_e of ~15 μm [*Painemal and Zuidema*, 2011]. The fundamental cause for the initiation of rain near 15 μm can be explained by the collection kernel coefficient that was found to be proportional to $r_e^{4.8}$ [*Freud and Rosenfeld*, 2012]. This power dependency means that the collection efficiency increases dramatically with r_e, so that above ~15 μm drizzle and raindrops are being created very quickly.

The geometrical cloud depth, D, was obtained by comparing the satellite retrieved LWP to the calculated adiabatic LWP and the corresponding height at which it is reached. Only satellite pixels with optical thickness larger than the 85th percentile were included because we assume that these pixels represent the deepest and most active clouds, which are more closely satisfying the adiabatic assumption.

The relationship between cloud depth, effective radius, and droplet number concentration is explained in *Freud and Rosenfeld* [2012] as follows: (a) adiabatic water increases nearly linearly with height for warm shallow clouds, which are the subject of this study, following the relation below:

$$q_{L_a} \propto D^b \qquad (1)$$

where D is cloud depth above its base and b is related to the exponent that fits best the dependence of the adiabatic cloud water on D, which is nearly 1 for warm shallow clouds. (b) The adiabatic cloud water content is proportional to the r_e in the power of 3 times the number of activated CCN at cloud base, N_a (based on the equation for spherical volume) as shown here:

$$q_{L_a} \propto {r_e}^3 N_a \tag{2}$$

Taking equations (1) and (2) together yields

$$D \propto \left(r_e^3 \ N_a\right)^{\frac{1}{b}} \tag{3}$$

Equation (3) means that for any r_e, D changes nearly linearly with N_a. A particular case of interest is when r_e equals to r_{ec}, the critical r_e for initiation of drizzle, which gives the theoretical critical cloud depth for initiation of significant drizzle, D_c as written here:

$$D_c \propto \left(r_{ec}^3 \ N_a\right)^{\frac{1}{b}} \tag{4}$$

By assuming that N_a equals to N_d, we calculated D_c in which r_{ec} is equals to 15 µm, where heavy drizzle should already start forming. The sensitivity of the calculation of D and D_c to the accuracy of the cloud base temperature and pressure is very small for MSC as analyzed here (i.e., shallow warm clouds). A change of 1 degree of cloud base temperature causes a change of about 30 m in D and D_c. A change of 100 mb in cloud base pressure causes even smaller change.

We chose three areas for the tracking analysis. The areas are shown by the polygons in Figure 3. Two of them are located within the continental cloud field and one within the maritime cloud field. The retrieval of the cloud parameters was available for the noon time each day. During nighttime retrievals are not available. Around sunrise and sunset the uncertainty of the retrievals is too high and therefore were not used.

3.5.1. Documentation of the Closed to Open Cells Process

3.5.1.1. The Role of Aerosol Scavenging

Figure 8 shows 3 days Lagrangian analysis of the microphysical, macrophysical, and meteorological parameters of an area of closed cells that formed within the continental air mass. The specific tracked area (Figure 8a) is shown by polygon a in Figure 3. The analyzed area ranged between ~4000 pixels at the early stage when the closed cells area was the largest, to about ~1500 pixels for the latest stage when the closed cell area became small just before breaking up. The pixel size at these latitudes is about 3.5 × 5.5 km. Note that retrieval errors are minimized over homogeneous cloud fields as analyzed here [*Zhang and Platnick*, 2011].

The real and critical cloud depth, D and D_c, are shown by the blue and red lines in Figure 8b. It can be seen that D_c changes with N_d (i.e., aerosol concentrations). This is in accordance with *Freud and Rosenfeld* [2012] (equation (4)) and explains the reason for the parallel slopes of the curves of D_c and N_d in Figure 8b. The beginning of significant drizzle and the following breakup of the closed cells occur when D exceeds D_c, as shown by the intersection of the blue and red lines. This is evident also by the observed r_e that exceeds 15 µm at the same time, as shown by the orange line in Figure 8b. Following this, as long as aerosols increase N_d and cause D_c to be greater than D, as in the presented case study, the rain is suppressed along with the delayed transition to open cells. *Bretherton et al.* [2010] showed that gradient in precipitation in the south east Pacific Ocean is related to deeper boundary layer and deeper clouds far off shore while *Terai et al.* [2012] further showed that the precipitation is also modulated by aerosols concentrations, in addition to cloud depth. These can be explained by the relation between D and D_c as described above.

The rate of the cleansing process of the clouds can be inferred by the decrease of N_d (Figure 8b). N_d is observed to decrease moderately during the first 2 days and then to decrease rapidly toward much lower values along with the opening of the closed cells. The abrupt decrease of N_d occurs due to the initiation of heavy drizzle that leads to an even faster scavenging of the aerosols in a positive feedback loop, causing the transition from closed to open cells [*Rosenfeld et al.*, 2006]. This is in fact the transition from the updraft limited to the aerosol limited regime following *Reutter et al.* [2009].

Figure 8c illustrates the maritimization process. The clouds form as closed cells just below the inversion base, driven by radiative cooling from the cloud tops [*Agee et al.*, 1973]. The closed cells thicken with time until

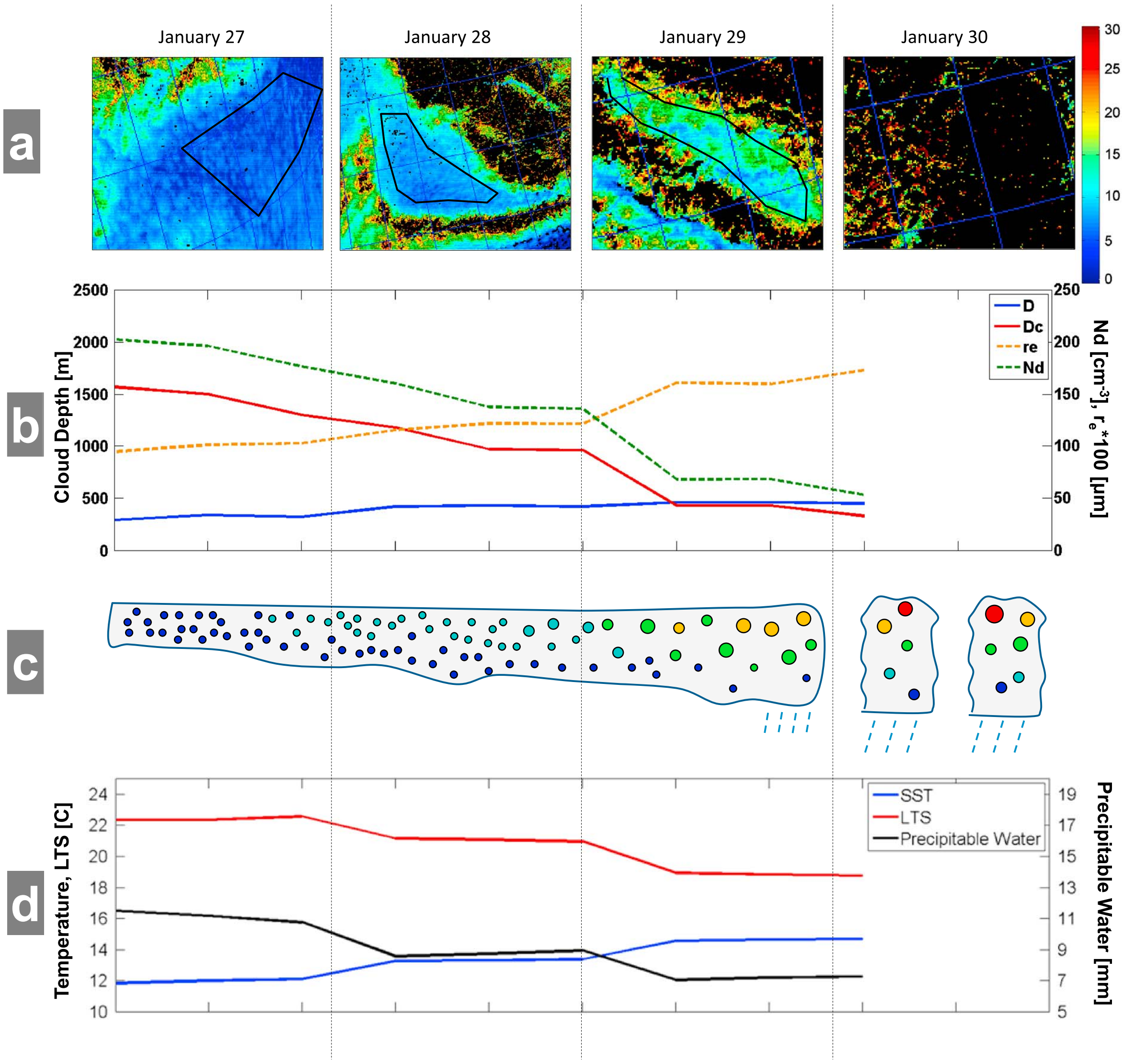

Figure 8. Lagrangian analysis and schematic illustration of the closed cells within polygon a that is shown in Figure 3. The vertical lines delimit the days. *D* represents the actual cloud depth, and D_c is the critical cloud depth that would initiate significant drizzle (i.e., at 15 μm). (a) The tracked polygons colored by MODIS r_e scale of 0–30 μm. (b) Three day evolution of the MSG-retrieved D (blue), D_c (red), r_e (orange), and N_d, (green) for the tracked closed cells. By 30 January the tracked closed cells broke up. Because retrievals over broken clouds are not reliable under the coarse resolution of the MSG the data for the 30 of January is not shown. Note that the closed cells open when the actual cloud depth, *D*, exceeds the threshold cloud depth for initiation of precipitation, D_c, shown by the intersection of the blue and red lines. (c) Illustration of the quantities shown in Figure 8b, showing the evolution of the transitioning process from closed to open cells. The cloud drops are colored according to their size with the color scale of the r_e in Figure 8a. (d) The change of the sea surface temperature, lower tropospheric stability (LTS), and precipitable water within the tracked area along the 3 days.

drizzle is sufficient enough for fast scavenging of the aerosols. The increased fluxes from the ocean surface due to the cold pools that reach the surface, and collisions between the cold pools, organize the convection in the form of open cells [*Feingold et al.*, 2010; *Rosenfeld et al.*, 2006; *Terai and Wood*, 2013; *Wang and Feingold*, 2009; *Yamaguchi and Feingold*, 2014]. Modeling and observational studies [*Terai et al.*, 2014; *Wang and Feingold*, 2009; *Wood et al.*, 2011] show similar pattern in which the closed cells become thicker along the transition to open cells.

3.5.1.2. The Role of Meteorology

Meteorological factors affect the depth of the MBL and thereby the cloud ability to deepen up to the height at which the necessary r_e for heavy drizzle is reached. Changes in SST can affect the stability of the MBL and

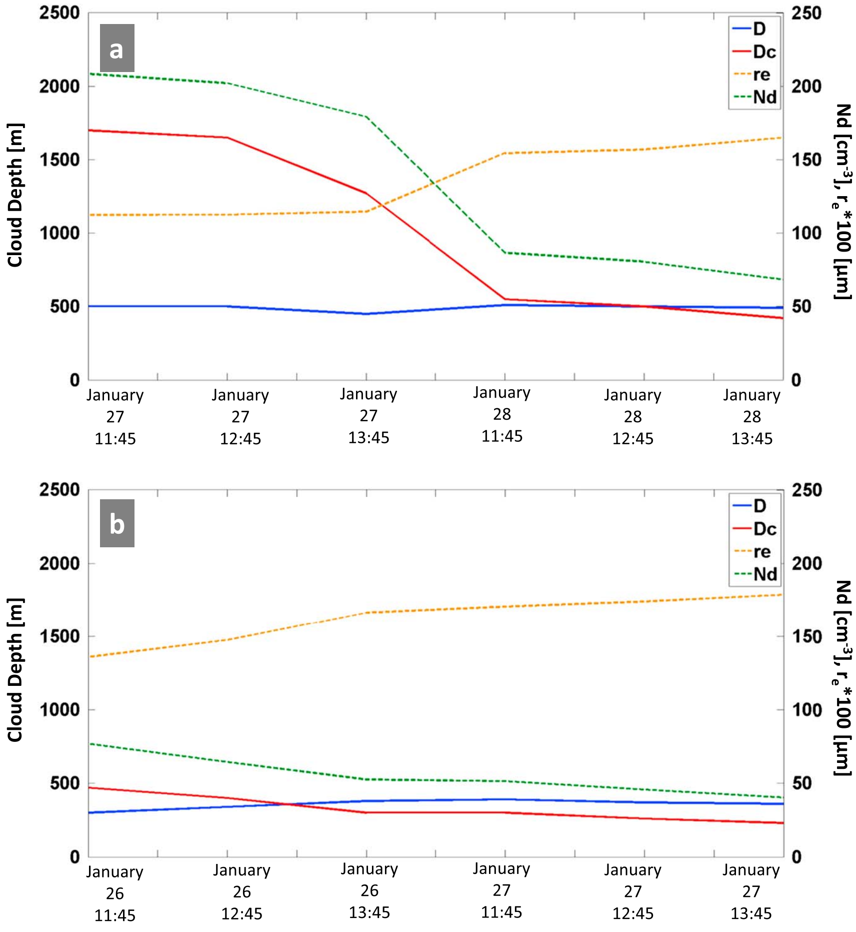

Figure 9. Lagrangian analysis of the closed cells in polygons b and c that are shown in Figure 3. (a) Plot (area b) is within the continental closed cells and its behavior is similar to area a (see Figure 8). (b) Plot (area c) is within the maritime closed cells and is observed to break to open cells at the first day. Note the difference in N_d and cloud depth between the two areas. The clouds break to open cells when D reaches D_c.

thus promote drizzle and breaking up of the closed cells. Therefore, in order to represent these factors, we documented the SST, lower tropospheric stability (LTS), and precipitable water above the inversion, as shown in Figure 8d. LTS is regarded as the strength of the inversion that caps the MBL and is calculated by the difference in the potential temperature between 700 hPa and the surface [*Wood and Hartmann*, 2006]. LTS is observed to decrease along the days until the breaking up of the closed cells. The decrease in LTS is not because of weakening of the high pressure and the subsidence above, but rather due to increasing SST and subsequently the surface air temperature (Θ_{700} increases with time, not shown). The observed decrease of the precipitable water above the inversion indicates that the high pressure is being more and more established. Lower precipitable water means that the radiative cooling, which is required for the maintenance of closed cell, becomes even stronger. Despite this, the closed cell break to open cells at this point, showing the dominant role of the aerosols.

The analysis here, which accounts for both the cloud microstructure and the meteorological factors that accompany the breaking process of the closed cells, allows to separate the impacts of these two factors that control the MSC regime changes.

Similar analysis to the above, but for two additional areas, is shown in Figures 9a and 9b. Figure 9a shows 2 days evolution of area b (see Figure 3) that is located within the continental closed cells and is more mature than area a by about half a day. Due to lack of temporal resolution during sunrise, sunset and nighttime, we cannot tell whether the change in r_e and N_d is rapid as shown in the Figure. However, sparse measurements can only show lower rate than the real one. The area of closed cells do not remain as isolated area of closed cells as area a. Instead, it breaks one day earlier to pockets of open cells that eventually overtake the whole area. Interestingly, the closed cells break when N_d reaches a value of ~75 cm^{-3} in both areas a and b. This is so because the cloud depths are similar (±50 m). Why area a remains as isolated closed cells while area b breaks earlier? Area a is located in the eastern part of the closed cells deck that was formed; hence, it is reasonably that it will survive longer because it formed at a later stage. It is also possible that it has higher aerosol concentrations; however, we cannot support that with our observations. In addition, the mechanism of cloud thickening at preferred locations can also explain the difference (see section 3.5.1.3), as evidence by the slightly thicker clouds in area b compare to area a (area b is thicker by about 50 m).

Figure 9b shows 2 day evolution of area c (see Figure 3) that exists within the maritime air mass. These closed cells are newly formed as they were observed to be created during the night before the analysis begins. The closed cells break to open cells during the first day, less than 24 h after their creation. This is possible given the low N_d and high r_e. Note that the theoretical cloud depth that is required for r_e to reach 15 μm, D_c, is much shallower in these clouds (500 compare to 1700 m in area b). Despite the shallow actual cloud depth, the low D_c (due to low N_d) allows significant drizzle to form and break the closed cells.

3.5.1.3. The Role of Cloud Deepening Due to Surface Convergence

In Figure 3e a strip of open cells is seen south of area a. Tracking back in time the origins of this band reveals that the unique shape of these pocket of open cells formed due to surface convergence during the night before. In Figure 3d, which shows the night before the appearance of the open cells band, a strip with darker purple color is seen south east of area a, implying that the clouds in this area have larger r_e. This can be caused by thickening of the clouds along that strip due to a convergence zone. We hypothesize that the convergence was caused by the confluence of a north-easterly flow that came from the British Islands with westerly flow that came from the Iberian peninsula (refer to the animated sequence in Movies S1 and S2 in which the clouds movement can be seen).

We used EUMETSAT atmospheric motion vectors (AMV) product to analyze the movement of the clouds in this area, for pin pointing the convergence line. Figure 10 shows the AMV for the night between the 27 and 28 of January overlaid the night microphysics imageries. It can be seen that the clouds follow the large-scale flow as was described above. We interpret the pattern in the large-scale flow as horizontal wind confluence in the area where the open cells formed later (shown by the boxes in Figure 10). The surface convergence is assumed to be responsible to the deeper clouds with the larger cloud top r_e and drizzle that broke the closed cells in the following day (Figure 10d). Calculation of the cloud depth in this area results with depth that is larger by 80 m compared to the clouds to the north (480 versus 400 m). The above analysis demonstrates the role of cloud deepening due to large scale meteorology that leads to breaking up of closed cells despite elevated aerosol concentrations. It can explain features of pockets of open cells that are often seen during cold polar outbreaks.

3.6. Cloud Radiative Effect

The CRE is defined as the difference in solar reflected radiation between the cloudy and cloud-free situations at the same time and place. We calculated the solar CRE between the open and closed cells that are seen in Figure 3e across the two sides of the interface line. The closed cells exist within the continentally polluted air mass while the open cells exist within the pristine air mass. The CRE over the closed cells was calculated to be about 50 Wm^{-2} in excess of the nearby open cells. Note that the calculated CRE is for the winter time when the solar radiation is near its annual minimum. The CRE for the same clouds can be almost four times larger during the summer and reach −195 Wm^{-2} in the northern hemisphere solstice day. We also applied the method that was presented by *Goren and Rosenfeld* [2014] to separate the contribution of the cloud cover, cloud LWP, and Twomey effects. The partitioning method relates the CRE between the open and closed cells to be 21% due to the Twomey effect, 35% due to the cloud cover effect, and 44% due to the cloud LWP effect. The cloud cover and cloud LWP effects reflect the cloud dynamical changes between the open and closed cells regimes and contribute together nearly 80% of the CRE.

As shown in section 3.3, it is likely that anthropogenic aerosols are responsible to the observed closed cells. Without the additional anthropogenic aerosols, those closed cell would probably break to open cells sooner. Therefore, part of the CRE can be considered here as RF. Quantifying the RF requires additional study.

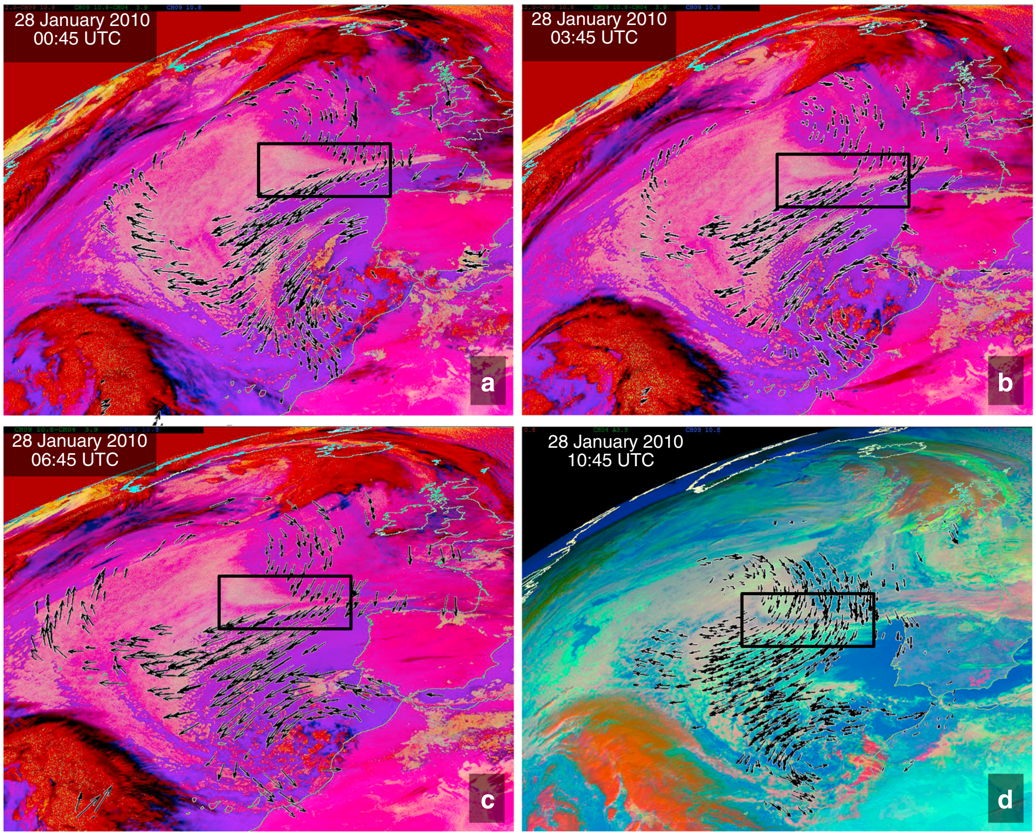

Figure 10. Atmospheric motion vectors retrieved from clouds at the lower atmosphere overlaid (a–c) night microphysics and (d) day microphysics imageries for selected times during the first half of 28 January. Figure 10d shows more arrows due to better day time retrieval. The largest arrows represent wind speed at 20 m/s. The airflow around the anticyclone can be seen west of Europe. Also note the cyclone south west of the Iberian peninsula. The boxes represent the area of interest. Note the wind confluence and a band of darker colored clouds where the wind shifts in Figures 10a–10c. The darker colors mean deeper clouds (see explanation for the color scheme in section 2). In Figure 10d a band of open cells is seen in the area where the convergence occurred (refer also to Figure 3e for better visualization of the clouds).

4. Discussion and Conclusions

Satellite snapshots frequently show patterns of open and closed cells with little indication for their origins, except for linear ship tracks. *Goren and Rosenfeld* [2012] have shown that ship tracks can expand and merge to form vast area of closed cells in the size of about 600 × 600 km. In this study we further show that continents can act as huge ships with respectively large tracks that form vast areas of closed cells downwind the continents when favorable meteorological conditions for MSC exist. The closed cells are observed to undergo a maritimization process, i.e., a cleansing process that involves transition from continentally polluted closed cells to maritime clean and precipitating open cells. The analysis shows that meteorology and SST variations do not explain the cloud regime transitions in the analyzed case study. The transitions are controlled by the different aerosol concentrations within the air masses in which the clouds exist. The documentation of the cleansing rate that we show here is important regardless whether the aerosols are natural or anthropogenic. It should be noted that in this study we present in-depth analysis for only one case, although we have observed several similar situations (see the supporting online material).

The analyses further shows that cloud droplet concentration, N_d, is a good parameter that can quantify the maritimization process. This is so because the cloud depth at which r_e exceeds the threshold for significant drizzle increases linearly with N_d [*Freud and Rosenfeld*, 2012]. Simulations of MSC support the hypothesis that precipitation plays a critical role in the formation and evolution of open cells and that lowering N_d to a value that allows significant drizzle for a cloud with a given depth can bring the transition from closed to open cells [*Wang and Feingold*, 2009; *Rosenfeld et al.*, 2012]. Following this, the maritimization process can be separated into three stages with respect to the dependence of N_d on time: (1) A slowly decreasing high N_d. This is expected to be observed initially in polluted air masses because N_d reaches saturation with respect to CCN (the updraft limited regime of *Reutter et al.* [2009]), so that a decrease of CCN concentrations due to collisions and coalescences is not manifested in a significant decrease in N_d. (2) An accelerating decrease of N_d. At this stage most of the additional interstitial CCN were scavenged and thus N_d can be decreased through collisions and coalescence processes. In this stage the clouds transition from the updraft limited to the aerosol limited regime [*Reutter et al.*, 2009]. (3) A rapid decrease of N_d and breakup into open cells. An abrupt decrease of N_d to very low values can occur due to the initiation of heavy drizzle that leads to an even faster scavenging of the aerosols in a positive feedback loop, causing the sharp transition from closed to open cells [*Rosenfeld et al.*, 2006]. This maritimazation process with its stages is illustrated in Figure 8. In accordance to previous studies [*Rosenfeld et al.*, 2006; *Sharon et al.*, 2006; *Stevens et al.*, 2005; *Wood et al.*, 2008, 2011; *Terai et al.*, 2014], Figure 8 demonstrates that aerosols can delay the initiation of the drizzle that is responsible to the transition to open cells, and thus increase the life time of closed cells. This is the aerosol indirect cloud life time effect [*Albrecht*, 1989].

The large-scale meteorology also plays a role in controlling the life time of the closed cells by governing the depth of the clouds, and thus, their possibility to produce drizzle. In that manner, given an amount of aerosols, the thinner closed cells would remain closed for longer time. This raise the importance of studying how would the MBL depth under the subtropical heights be change in the future. Shallower MBL will tend to increase the cloud life time effect while deeper MBL will moderate it. This is in accordance with *Terai et al.* [2012] who showed that the precipitation susceptibility in MSC decreases with increasing cloud thickness.

Aerosol CRE can be referred as RF when anthropogenic aerosols are responsible to changes in the CRE over a specific area. These changes can be due to the Twomey, cloud cover, and cloud life time effects. We show that it is possible that the added CRE of closed cells as those studied here is in fact RF, mainly caused by the cloud life time and cover effects. We suggest that it is quite possible that at least part of the areas of closed MSC that are frequently seen over the subtropical oceans may be mostly or fully cloudy due to anthropogenic pollution, thus potentially causing to a much larger cloud cover effect than estimated from observations and climate models. These closed MSC can be termed "continental tracks," in analogy to ship tracks, but at a much larger scale. It should be noted that in this paper we did not aim to estimate the climatological significance of such cases, as this requires further study. This study shows a mechanism for a potentially hitherto unrecognized large negative RF over very large area for long time. If this is a common occurrence, it implies a major climate impact that is yet not taken into account.

Acknowledgments
The GOCART model output is provided by Mian Chin at NASA Goddard Space Flight Center, which was produced under the support of NASA MAP and ACMAP programs. The satellite and reanalysis data that were used in this study are available to download per request by the ordering data systems: MSG (https://eoportal.eumetsat.int/userMgmt/login.faces), MODIS (http://ladsweb.nascom.nasa.gov/data/search.html), CALIPSO (http://reverb.echo.nasa.gov/); CloudSat (http://www.cloudsat.cira.colostate.edu/), NCEP/NCAR reanalysis (http://www.esrl.noaa.gov/psd/data/ gridded/data.ncep.reanalysis.html), and ECMWF (http://www.ecmwf.int/). Carbon monoxide concentrations can be downloaded at http://agage.eas.gatech.edu/data_archive/agage/gc-md/complete/macehead/. Further detailed information describing data products that were used can be found in section 2. This study was supported by the EU program BACCHUS FP7-603445. The authors thank to Joerg Trentmann and Anke Kniffka from the Deutscher Wetterdienst for assitance with obtaining the SEVIRI cloud products. The authors also thank to Carynelisa Erlick who set up the radiative transfer algorithm for the CRE calculations.

References

Agee, E. M., T. S. Chen, and K. E. Dowell (1973), A review of mesoscale cellular convection, *Bull. Am. Meteorol. Soc.*, *54*(10), 1004–1012.
Albrecht, B. A. (1989), Aerosols, cloud microphysics, and fractional cloudiness, *Science*, *245*(4923), 1227–1230.
Allen, G., et al. (2011), South East Pacific atmospheric composition and variability sampled along 20°S during VOCALS-REx, *Atmos. Chem. Phys.*, *11*(11), 5237–5262.
Atkinson, B. W., and J. W. Zhang (1996), Mesoscale shallow convection in the atmosphere, *Rev. Geophys.*, *34*(4), 403–431, doi:10.1029/96RG02623.
Benkovitz, C. M., M. T. Scholtz, J. Pacyna, L. Tarrasón, J. Dignon, E. C. Voldner, P. A. Spiro, J. A. Logan, and T. E. Graedel (1996), Global gridded inventories of anthropogenic emissions of sulfur and nitrogen, *J. Geophys. Res.*, *101*(D22), 29,239–29,253, doi:10.1029/96JD00126.
Boucher, O., and U. Lohmann (1995), The sulfate-CCN-cloud albedo effect, *Tellus B*, *47*(3), 281–300.
Bretherton, C. S., R. Wood, R. C. George, D. Leon, G. Allen, and X. Zheng (2010), Southeast Pacific stratocumulus clouds, precipitation and boundary layer structure sampled along 20°S during VOCALS-REx, *Atmos. Chem. Phys.*, *10*(21), 10,639–10,654.
Chin, M., and D. J. Jacob (1996), Anthropogenic and natural contributions to tropospheric sulfate: A global model analysis, *J. Geophys. Res.*, *101*(D13), 18,691–18,699, doi:10.1029/96JD01222.
Chin, M., et al. (2014), Multi-decadal aerosol variations from 1980 to 2009: a perspective from observations and a global model, *Atmos. Chem. Phys.*, *14*(7), 3657–3690.
Draxler, R. R. and Rolph, G. D. (2015), HYSPLIT (HYbrid Single-Particle Lagrangian Integrated Trajectory) model access via NOAA ARL READY website. [Available at http://ready.arl.noaa.gov/HYSPLIT.php], NOAA Air Resources Lab., Silver Spring, Md.
Feingold, G., I. Koren, H. Wang, H. Xue, and W. A. Brewer (2010), Precipitation-generated oscillations in open cellular cloud fields, *Nature*, *466*(7308), 849–852.
Feingold, G., I. Koren, T. Yamaguchi, and J. Kazil (2015), On the reversibility of transitions between closed and open cellular convection, *Atmos. Chem. Phys. Discuss.*, *15*(4), 5553–5588.

Field, C., V. Barros, D. Dokken, K. Mach, M. Mastrandrea, T. Bilir, M. Chatterjee, K. Ebi, Y. Estrada, and R. Genova (2014), *IPCC, 2014: Climate Change 2014: Impacts, Adaptation, and Vulnerability. Part A: Global and Sectoral Aspects. Contribution of Working Group II to the Fifth Assessment Report of the Intergovernmental Panel on Climate Change*, Cambridge Univ. Press, Cambridge, U. K., and New York.

Freud, E., and D. Rosenfeld (2012), Linear relation between convective cloud drop number concentration and depth for rain initiation, *J. Geophys. Res.*, *117*, D02207, doi:10.1029/2011JD016457.

George, R. C., and R. Wood (2010), Subseasonal variability of low cloud radiative properties over the southeast Pacific Ocean, *Atmos. Chem. Phys.*, *10*(8), 4047–4063.

George, R. C., R. Wood, C. S. Bretherton, and G. Painter (2013), Development and impact of hooks of high droplet concentration on remote southeast Pacific stratocumulus, *Atmos. Chem. Phys.*, *13*(13), 6305–6328.

Gerber, H. (1996), Microphysics of marine stratocumulus clouds with two drizzle modes, *J. Atmos. Sci.*, *53*(12), 1649–1662.

Goren, T., and D. Rosenfeld (2012), Satellite observations of ship emission induced transitions from broken to closed cell marine stratocumulus over large areas, *J. Geophys. Res.*, *117*, D17206, doi:10.1029/2012JD017981.

Goren, T., and D. Rosenfeld (2014), Decomposing aerosol cloud radiative effects into cloud cover, liquid water path and Twomey components in marine stratocumulus, *Atmos. Res.*, *138*, 378–393.

Kaufman, Y. J., I. Koren, L. A. Remer, D. Rosenfeld, and Y. Rudich (2005), The effect of smoke, dust, and pollution aerosol on shallow cloud development over the Atlantic Ocean, *Proc. Natl. Acad. Sci. U.S.A.*, *102*(32), 11,207–11,212.

Lebsock, M. D., G. L. Stephens, and C. Kummerow (2008), Multisensor satellite observations of aerosol effects on warm clouds, *J. Geophys. Res.*, *113*, D15205, doi:10.1029/2008JD009876.

Lensky, I. M., and D. Rosenfeld (2008), Clouds-Aerosols-Precipitation Satellite Analysis Tool (CAPSAT), *Atmos. Chem. Phys.*, *8*(22), 6739–6753.

Lu, M. L., W. C. Conant, H. H. Jonsson, V. Varutbangkul, R. C. Flagan, and J. H. Seinfeld (2007), The Marine Stratus/Stratocumulus Experiment (MASE): Aerosol-cloud relationships in marine stratocumulus, *J. Geophys. Res.*, *112*, D10209, doi:10.1029/2006JD007985.

Marchand, R., G. G. Mace, T. Ackerman, and G. Stephens (2008), Hydrometeor Detection Using Cloudsat—An Earth-Orbiting 94-GHz Cloud Radar, *J. Atmos. Ocean. Technol.*, *25*(4).

Painemal, D., and P. Zuidema (2011), Assessment of MODIS cloud effective radius and optical thickness retrievals over the Southeast Pacific with VOCALS-REx in situ measurements, *J. Geophys. Res.*, *116*, D24206, doi:10.1029/2011JD016155.

Platnick, S., M. D. King, S. A. Ackerman, W. P. Menzel, B. A. Baum, J. C. Riedi, and R. A. Frey (2003), The MODIS cloud products: Algorithms and examples from Terra, *IEEE Trans. Geosci. Remote Sens.*, *41*(2), 459–473.

Rangno, A. L., and P. V. Hobbs (2005), Microstructures and precipitation development in cumulus and small cumulonimbus clouds over the warm pool of the tropical Pacific Ocean, *Q. J. Roy. Meteorol. Soc.*, *131*(606), 639–673.

Reutter, P., H. Su, J. Trentmann, M. Simmel, D. Rose, S. Gunthe, H. Wernli, M. Andreae, and U. Pöschl (2009), Aerosol-and updraft-limited regimes of cloud droplet formation: influence of particle number, size and hygroscopicity on the activation of cloud condensation nuclei (CCN), *Atmos. Chem. Phys.*, *9*(18), 7067–7080.

Rolph, G. D. (2015), Real-time Environmental Applications and Display sYstem (READY) website. [Available at http://ready.arl.noaa.gov], NOAA Air Resources Lab., Silver Spring, Md.

Rosenfeld, D., Y. J. Kaufman, and I. Koren (2006), Switching cloud cover and dynamical regimes from open to closed Benard cells in response to the suppression of precipitation by aerosols, *Atmos. Chem. Phys.*, *6*, 2503–2511.

Rosenfeld, D., H. L. Wang, and P. J. Rasch (2012), The roles of cloud drop effective radius and LWP in determining rain properties in marine stratocumulus, *Geophys. Res. Lett.*, *39*, L13801, doi:10.1029/2012GL052028.

Saide, P., S. Spak, G. Carmichael, M. Mena-Carrasco, Q. Yang, S. Howell, D. Leon, J. R. Snider, A. R. Bandy, and J. L. Collett (2012), Evaluating WRF-Chem aerosol indirect effects in Southeast Pacific marine stratocumulus during VOCALS-REx, *Atmos. Chem. Phys.*, *12*(6).

Schwartz, S., E. Harshvardhan, and C. M. Benkovitz (2002), Influence of anthropogenic aerosol on cloud optical depth and albedo shown by satellite measurements and chemical transport modeling, *Proc. Natl. Acad. Sci. U.S.A.*, *99*(4), 1784–1789.

Sekiguchi, M., T. Nakajima, K. Suzuki, K. Kawamoto, A. Higurashi, D. Rosenfeld, I. Sano, and S. Mukai (2003), A study of the direct and indirect effects of aerosols using global satellite data sets of aerosol and cloud parameters, *J. Geophys. Res.*, *108*(D22), 4699, doi:10.1029/2002JD003359.

Sharon, T. M., B. A. Albrecht, H. H. Jonsson, P. Minnis, M. M. Khaiyer, T. M. van Reken, J. Seinfeld, and R. Flagan (2006), Aerosol and cloud microphysical characteristics of rifts and gradients in maritime stratocumulus clouds, *J. Atmos. Sci.*, *63*(3), 983–997.

Spiro, P. A., D. J. Jacob, and J. A. Logan (1992), Global inventory of sulfur emissions with 1°×1° resolution, *J. Geophys. Res.*, *97*(D5), 6023–6036, doi:10.1029/91JD03139.

Stevens, B., G. Vali, K. Comstock, R. Wood, C. van Zanten, P. H. Austin, C. S. Bretherton, and D. H. Lenschow (2005), Pockets of open cells and drizzle in marine stratocumulus, *Bull. Am. Meteorol. Soc.*, *86*, 51–57.

Szczodrak, M., P. H. Austin, and P. B. Krummel (2001), Variability of optical depth and effective radius in marine stratocumulus clouds, *J. Atmos. Sci.*, *58*(19), 2912–2926.

Terai, C., and R. Wood (2013), Aircraft observations of cold pools under marine stratocumulus, *Atmos. Chem. Phys.*, *13*(19), 9899–9914.

Terai, C. R., R. Wood, D. C. Leon, and P. Zuidema (2012), Does precipitation susceptibility vary with increasing cloud thickness in marine stratocumulus?, *Atmos. Chem. Phys.*, *12*(10), 4567–4583.

Terai, C., C. Bretherton, R. Wood, and G. Painter (2014), Aircraft observations of five pockets of open cells sampled during VOCALS REx, *Atmos. Chem. Phys. Discuss.*, *14*(6), 8287–8332.

Twohy, C. H., J. A. Coakley, Jr., and W. R. Tahnk (2009), Effect of changes in relative humidity on aerosol scattering near clouds, *J. Geophys. Res.*, *114*, D05205, doi:10.1029/2008JD010991.

Twomey, S. (1974), Pollution and the planetary albedo, *Atmos. Environ. (1967)*, *8*(12), 1251–1256.

Twomey, S. (1977), The Influence of Pollution on the Shortwave Albedo of Clouds, *J. Atmos. Sci.*, *34*(7), 1149–1152.

Wang, H. L., and G. Feingold (2009), Modeling mesoscale cellular structures and drizzle in marine stratocumulus. Part II: The microphysics and dynamics of the boundary region between open and closed cells, *J. Atmos. Sci.*, *66*(11), 3257–3275.

Wood, R. (2005), Drizzle in stratiform boundary layer clouds. Part I: Vertical and horizontal structure, *J. Atmos. Sci.*, *62*(9), 3011–3033.

Wood, R., and D. L. Hartmann (2006), Spatial variability of liquid water path in marine low cloud: The importance of mesoscale cellular convection, *J. Clim.*, *19*(9), 1748–1764.

Wood, R., K. K. Comstock, C. S. Bretherton, C. Cornish, J. Tomlinson, D. R. Collins, and C. Fairall (2008), Open cellular structure in marine stratocumulus sheets, *J. Geophys. Res.*, *113*, D12207, doi:10.1029/2007JD009371.

Wood, R., C. S. Bretherton, D. Leon, A. D. Clarke, P. Zuidema, G. Allen, and H. Coe (2011), An aircraft case study of the spatial transition from closed to open mesoscale cellular convection over the Southeast Pacific, *Atmos. Chem. Phys.*, *11*(5), 2341–2370.

Yamaguchi, T., and G. Feingold (2014), On the relationship between open cellular convective cloud patterns and the spatial distribution of precipitation, *Atmos. Chem. Phys. Discuss.*, *14*(18), 25,651–25,685.

Yang, Q., W. Gustafson Jr., J. D. Fast, H. Wang, R. C. Easter, H. Morrison, Y.-N. Lee, E. G. Chapman, S. Spak, and M. Mena-Carrasco (2011), Assessing regional scale predictions of aerosols, marine stratocumulus, and their interactions during VOCALS-REx using WRF-Chem, *Atmos. Chem. Phys.*, *11*(23), 11,951–11,975.

Zhang, Z., and S. Platnick (2011), An assessment of differences between cloud effective particle radius retrievals for marine water clouds from three MODIS spectral bands, *J. Geophys. Res.*, *116*, D20215, doi:10.1029/2011JD016216.